Characterization and Simulation of Tactile Sensors

Zachary Pezzementi*
Dept. of Computer Science
Johns Hopkins University

Erica Jantho
Dept. of Biomedical Engineering
Johns Hopkins University

Lucas Estrade
Dept. of Computer Science
Paul Sabatier University

Gregory D. Hager†
Dept. of Computer Science
Johns Hopkins University

ABSTRACT

The response of a tactile sensor system (consisting of the sensors themselves and the material covering them) was characterized via robotic experiments. A *point spread function* model of this response was developed for typical interaction forces, allowing the use of graphics and imaging techniques respectively for simulating and interpreting tactile sensor readings. This model was implemented in software as a generic artificial tactile sensor simulator, and its accuracy at approximating the output of our test system is demonstrated.

Index Terms: I.2.9 [Computing Methodologies]: Artificial Intelligence—Robotics; I.6.5 [Computing Methodologies]: Simulation and Modeling—Model Development

1 INTRODUCTION

Recognition of objects and/or control of object manipulation through tactile sensing has been a long-sought goal [1, 3, 9]. Tactile sensation is generally defined as any sensation associated with the skin, as opposed to force sensing, which instead originates in muscles and joints. For humans, this may include sensation of such phenomena as temperature, vibration, and surface roughness, due to the variety of sensors embedded in our skin. In this work (as in most of the prior work in robotics), we will focus on tactile sensation measured with array of force sensors, most closely resembling Merkel receptors [10] in the human system.

In the early work on haptic object recognition, tactile sensors were deemed inadequate for much more than determining contact vs. no contact [2], and were generally used only to localize contact point(s) on a fingertip [4]. Only recently have such tactile sensors become available at the level of precision and resolution one would want for recognition and manipulation tasks. Recent optically-based sensors, such as those presented in [11], boast impressive spatial resolutions, but are not yet widely available. They would also be difficult to incorporate into, say, a robot hand at present. Capacitive sensors, such as the ones used in this work, have made great strides in force resolution, but still have relatively low spatial resolution. Nonetheless, in [16], Yanagida et al. showed 87% accuracy for character recognition using a 3x3 grid of "tactile" displays, presented to a human subject's back via a chair, demonstrating the potential descriptiveness of even very low resolution tactile information.

A common theme to much of the prior work on tactile sensing has been to attempt to infer physical characteristics of the external world (i.e. location of contact or surface shape) from the sensor output.

For example, in [8], Fearing and Binford analyzed the sensitivity of a hemispherical tactile sensor for discriminating simple shaped indenters. Based on careful physical measurements, they modeled the effect of a compliant sensor covering using an impulse response function taking the form of a truncated quadratic. They then suggest the use of inverse filtering techniques to infer the actual surface contact structure. Others propose the use of SVD [7], neural nets [6], or radial basis functions [5] to the same end. However, any such approach is inherently ill-posed, as the associated deconvolution problem does not have a unique solution.

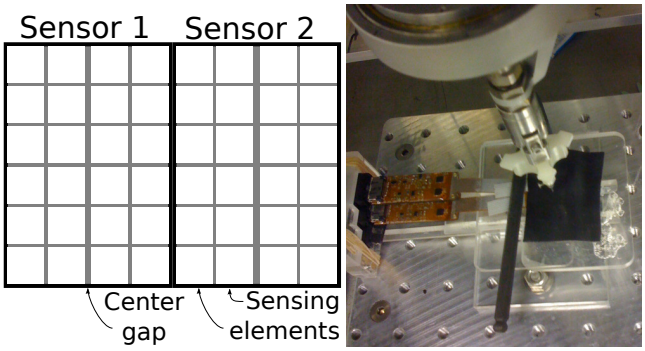

Figure 1: (a) Diagram of our sensing system consists of a 1-by-2 arrangement of sensors, each of which comprises a 6-by-4 array of 1.8mm square sensing elements. 0.2mm of (non-sensing) spacing is necessary between the individual sensors, except for the middle column of each sensor, where this gap is doubled. (b) The actual sensors mounted in the workspace of the robot with indenter.

In this paper, we instead take the view that a high resolution tactile sensor can be simply characterized as a device for producing tactile images, with no attempt to infer the physical causes of images. We first describe a general methodology for modeling the response characteristics of tactile sensors from empirical sensor data. As in [8], one of the key ideas is to develop and optimize a *point spread function* (PSF) model for tactile sensors from empirical sensor data. More specifically, tactile sensors are typically covered with a layer of a relatively soft, elastic material, such as rubber, both to protect the sensors and to increase the range of displacements that can be distinguished by the sensors. Since this covering will tend to spread the response of the sensor to an input stimulus, it offers an interesting trade-off between spatial resolution and force resolution. The current state of the art for modeling force-displacement characteristics of such systems is finite element analysis, which has been shown to be very accurate, but which is also computationally expensive. Since the deformation in our system is relatively simple, the vast majority of the motion restricted to one degree of freedom of a uniform, isotropic material, we show that PSF models suffice to capture the effects of deformation. These results then support the optimization of the PSF to have specific spatial and force resolution characteristics.

The use of PSF-based models allows us to re-cast the task of simulating tactile sensors as one of graphics rendering. We describe a simulation environment we have developed that supports rapid rendering of large-scale models, and show that this simulation produces images that are qualitatively similar to those obtained from the physical sensor. This in turn opens the door to a wealth

*e-mail: zap@cs.jhu.edu
†e-mail: hager@cs.jhu.edu

of techniques from computer vision and image processing, including image-based representations of surface "appearance", texture classification and description, and "tactile mosaicking."

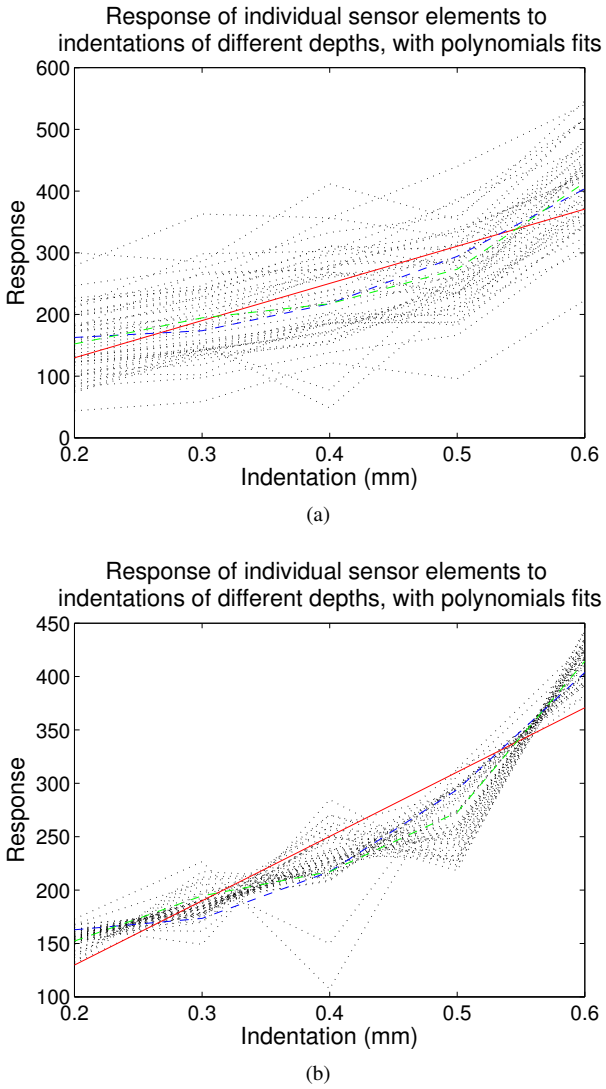

Figure 2: (a) Measured responses to displacements of different depths. (b) Re-calibration of the same values to a consistent linear fit. In both cases, dotted black lines give the response of individual sensor elements to a point load at varying indentation levels. The solid red line shows a linear fit to these values. The dashed blue line shows a quadratic fit.

2 Sensor System Force Characterization

The tactile sensor studies in this paper is a custom DigiTacts system from Pressure Profile Systems [12], consisting of two small sensors, each of which is 12mm-by-8.5mm and contains sensing elements with a spatial resolution of 1.8mm, for a total of 48 sensor elements making up an 8-x-6 "tactile image", as shown in Figure 1. The total sensor system footprint is 12mm-by-16.7mm, with 81% of the area being sensed, and the remaining 19% consisting of material between the individual sensing elements. The sensing modality was capacitive, with a sample rate of 30 Hz, sensitivity of 0.1 psi and a sensing range of 0-20 psi, though our interaction forces were restricted to the bottom of this range.

2.1 Force Response Testing

We first performed a set of tests to determine the linearity and uniformity of response across the sensors' surfaces. A robotic arm was programmed to press a cylindrical indentor (1mm diameter) into the center of each sensing element of the tactile sensor. The arm used was a custom-made platen-forcer system with a resolution of 3μm in the horizontal directions and 1μm in the vertical direction. To avoid damaging the sensors, a thin covering was used, consisting of 0.04" of polyurethane with a durometer rating of 40 OO (McMaster-Carr Part 8824T112).

The sensors were fixed to a flat surface within the robot arm's workspace. The arm's position was calibrated by pressing down on individual sensing elements to obtain a response which only excited a single element at a time (and no adjacent elements). The location of the elements was established in a calibration step where two points close to opposing corners of the sensor were measured to establish the sensor's orientation in the robot frame. The height of the surface of the covering in the vertical direction was measured at a single point and assumed to be uniform across the sensor. The robot then indented the rubber covering over each sensor element at the estimated center of the element, starting at the surface, and depressing incrementally by displacements of 0.2, 0.3, 0.4, 0.5, and 0.6 mm. For each indentation, the sensor readings over the 250 ms period of contact for each sensor element were averaged to get a single reading that was used for further processing.

2.2 Response Function

The overall response of the sensors was determined to be nearly linear in the range tested, though responses of individual sensing elements displayed some variation, as shown in Figure 2. This figure shows both a linear and a quadratic fit of response vs. indentation. We chose to use a linear model for interactions at the low end of this force range, but a quadratic model appears more appropriate for larger interaction forces. Two elements (one each located in the same corresponding position on each sensor) were omitted from this fit due to observed systematic errors. They responded to a stimulus of one adjacent element, but not to the element itself.

In all that follows, the force outputs were corrected by the per-pixel linear response model to obtain a more uniform response.

3 Point Spread Function

The layers of polyurethane covering the sensor tend to spread applied forces across the surface of the sensor, potentially exciting adjacent sensing elements even when a point force is applied. In this section, we model this process as a linear operator that is characterized by a point spread function.

Shimojo analyzed the low-pass filtering effects of tactile sensor coverings in [13], and fit models by finite element analysis that strongly resemble Gaussians. We also analyzed the interaction mechanics of the sensor covering by constructing a finite element model (FEM) to verify the accuracy of a Gaussian approximation. Since our primary interest was the output that would result on the sensor, we considered the FEM as a transfer function, taking an applied force on the top of the covering as input and producing forces at the bottom of the covering that are then measured by the sensing element. We investigated the covering's impulse response by applying a point load at the center of the top of the covering, while varying the covering thicknesses. As shown in Figure 3, the response predicted by the FEM closely resembles an exponential, and the width of that exponential appears to increase with the thickness of the covering. After the discretization inherent in array sensors, the FEM output and that of a Gaussian PSF are nearly identical, as illustrated in Figure 4. For this reason, we make use of Gaussian point spread functions in the remainder of this section. It should be noted that the FEM used a simple linear elastic deformation model, which can not be considered accurate for large deformations of such

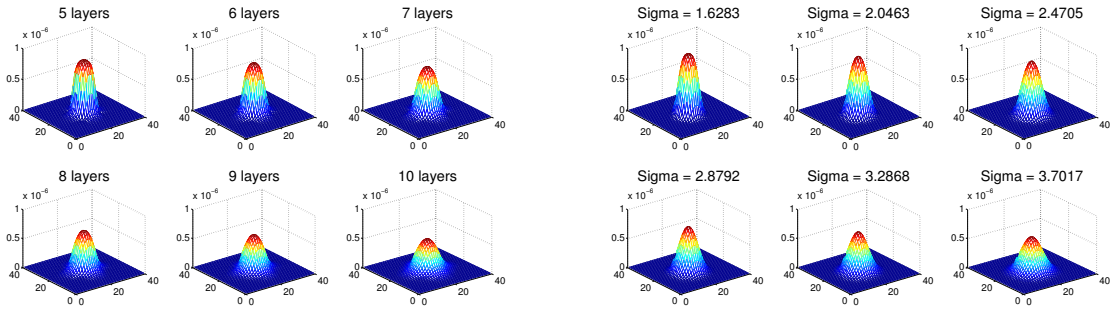

(a) (b)

Figure 3: (a) Finite element model prediction of impulse response of coverings of different thicknesses. The node forces at the center of the bottom layer of a 100x100 linear elastic FEM are shown when a point force is applied to the top center node. The number of vertical layers of elements in the model is varied from 5 to 10, giving the differently-shaped responses shown. (b) Convolution of the same input with a Gaussian with $\sigma = 0.5t + 0.9$

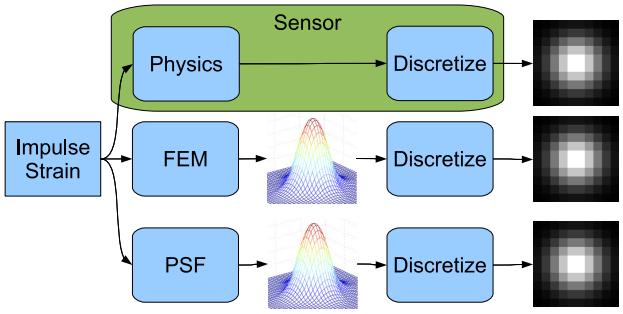

Figure 4: Different imaging models for tactile sensing. Nearly identical outputs can be obtained from a finite element model (FEM) or point spread function (PSF) model as from the actual sensor.

a material, but it nonetheless provided motivation to collect experimental data to verify this behavior.

3.1 Tests

The tests for characterizing the sensors' point spread function were designed to estimate the sensor's impulse response with different coverings, and to thereby identify the point spread function which best fit it. Since the sensor's resolution is relatively low, however, only a highly discretized version of the impulse response can be obtained from a single reading. This image does not have sufficient detail for an accurate fit. We overcame this limitation by acquiring multiple measurements with small translations between them.

The resulting set of tests was similar to that for the general response function. The same robot and indentation device were used as in the previous section. The indentations were spaced in a uniform 15-x-15 grid with a spacing of 0.1 mm between adjacent points. The grid was centered on one sensing element, so the resulting indentations fell at regular intervals across that element's entire extent, above the gaps between elements, and partially overlapped with each adjacent sensing element. The element used was chosen as one whose neighborhood exhibited low noise characteristics and seemed representative of the sensors' general response. This procedure was repeated for 4 different covering thicknesses, 0.04", 0.1", 0.14", and 0.2", built from 0.04" and 0.1" layers of the same polyurethane used in the force response tests. At each thickness, 3 indentation depths were tested, to determine whether the general response characteristics observed above still held as the covering thickness was increased. These depths were 30%, 50%, and 65% of each covering thickness.

3.2 Results

The sensors' impulse response was estimated from the data collected in Section 3 by fitting a rotationally symmetric Gaussian function to the data, varying its "spread" parameter, σ:

$$r = \sqrt{x^2 + y^2} \tag{1}$$

$$\mathbf{G}_\sigma(r) = \exp\left(-\frac{r^2}{2\sigma^2}\right) \tag{2}$$

Simulated input profiles, $\mathbf{I}_i$, $i = 1, 2, \ldots, 225$ were defined at high resolution, matching the shape and location of the robot indentation device used to collect sensor data. A candidate point spread function, $\mathbf{G}_\sigma$, corresponding to a particular choice of σ, was applied to this profile. The result was then normalized and down-sampled by a function, $\mathscr{S}$, to match the resolution of the actual sensor output, $\mathbf{D}_i$, accounting for gaps between sensing elements. The resulting simulated sensor reading is thus $\mathbf{E}_{i,\sigma} = \mathscr{S}(\mathbf{I}_i * \mathbf{G}_\sigma)$, where $*$ denotes convolution in the spatial domain. The correlation between measured and simulated images, $q_{i,\sigma} = < \mathbf{E}_i, \mathbf{D}_i >$, was used as the quality of fit metric for each image, and an overall quality of fit was computed as

$$Q(\sigma) = \sum_i q_{i,\sigma}. \tag{3}$$

The best-fit value, σ^+ was found by maximizing $Q(\sigma)$ over all values of σ.

σ^+ values for each thickness and indentation depth are shown in Figure 5a. A linear fit was applied to these points to derive an estimate of σ^+ as a function of covering thickness, t, both expressed in sensor element widths. The result is:

$$\sigma^+ \approx 1.11 + 0.497t \tag{4}$$

Exemplar PSFs with σ values from this equation for each covering thickness are shown in Figure 5b. The large value of the intercept of Equation 4 is likely due to the fact that the sensor has an inherent point spread function itself, even without a covering applied.

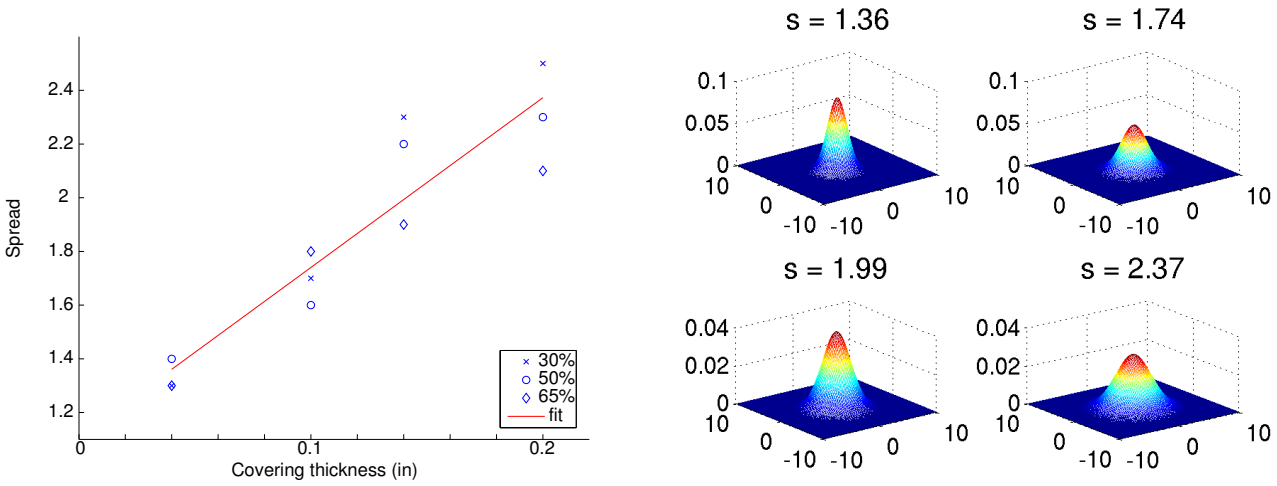

(a) (b)

Figure 5: (a) Point spread function spread parameter vs covering thickness, with polynomial fits, linear in red and quadratic in green. (b) Exemplar point spread functions with the parameters of the data 30% indentation level at each covering thickness.

4 Optimizing for Spatial Acuity

A simple model of the sensor's discretization processes was developed to analyze the optimal covering thickness to use to maximize spatial acuity. A discretizing sensor was considered to be defined by a function, $\mathbf{S}_{\mathbf{w},\mathbf{f}}(\mathbf{X})$ of spatial resolution (sensor element width $\mathbf{w}$) and force resolution ($\mathbf{f}$) given by

$$\mathbf{S}_{\mathbf{w}_i} = \int_i \mathbf{X} \tag{5}$$

$$\mathbf{S}_{\mathbf{w}_i,\mathbf{f}} = \lfloor \mathbf{S}_{\mathbf{w}_i} + 0.5\mathbf{f} \rfloor \tag{6}$$

This function takes the continuous input function, $\mathbf{X}$, representing force over the area of the sensor, and outputs a discretized version akin to the digital output of our sensors. Spatial discretization is accomplished by integrating the force profile, $\mathbf{X}$, over the area of each sensing element, representing the computation of the total resolved force acting in the measured direction. Force discretization consists of rounding the result to the nearest multiple of $\mathbf{f}$. For simplicity, the input and output of $\mathbf{S}$ were defined to be one-dimensional. The output range was chosen to comprise a number of sensor elements sufficient to describe the response to an impulse applied at any point on one sensing element, which for our purposes was 5.

The impulse response was modeled, as determined above, as a Gaussian function (centered at the point of application of the impulse, μ) with standard deviation, σ, increasing with the thickness of the covering:

$$\mathbf{G}_{\mu,\sigma}(x) = \frac{1}{\sigma\sqrt{2\pi}} \exp\left(-\frac{(x-\mu)^2}{2\sigma^2}\right) \tag{7}$$

We considered the performance on two tasks as criteria for measuring spatial acuity: spatial localization of a point force, and two point discrimination. In both cases, we searched for the optimum σ value with respect to sensor elements of width 1 unit, over different levels of force discretization.

For the spatial localization task, the goal is to identify the point at which a force was applied as closely as possible. Rather than choosing a particular estimation procedure, we instead consider an upper bound on feasible estimation accuracy. Let $\mathbf{r}_{\sigma,\mathbf{f}}$ be the number of distinct representations produced by a point force applied at every possible location within a single sensor element, that is the number of different sensor readings which would result from moving $\mathbf{G}$ from one end of an element to the other. This is an upper bound on performance in the following sense: If two inputs produce identical outputs, they can not possibly be differentiated, so the number of distinct outputs limits possible performance on the task, regardless of estimation method.

Intuitively, one would expect extreme values of σ to produce poor results: As σ approaches 0, G approaches an impulse, which excites only the sensor element it falls on and does not allow any inference about where within the element the force was applied based on the response of adjacent elements. At the other extreme, G approaches a uniform response across all sensor elements, which is even less informative. One would expect, therefore, that an optimal value lies somewhere in between.

A Gaussian input, $\mathbf{G}_{\mu,\sigma}$ was defined with μ initialized to 0, that is centered on the left edge of the central sensing element. μ was then increased in steps of $0.02\mathbf{f}$ units. Space and force discretization were applied, as in Equations 5-6, and the number of distinct sensor outputs was recorded for 25 values each of $\mathbf{f}$ and σ, drawn from a log scale. Figure 6a shows the (log of the) number of distinct representations produced by the procedure described above, while varying both the spread of the input and the level of discretization of the output force values. For all levels of force discretization, there is a prominent ridge in the graph around $\sigma \approx 0.3$.

We used a similar approach for the two point discrimination task. In this case, two Gaussian inputs were defined and initialized to the same location, so that the result (by superposition) is a single Gaussian of twice the amplitude. The two inputs were then gradually moved apart, maintaining the same center point, but increasing a separation distance in increments again of $0.02\mathbf{f}$ units. Again, space and force discretization were applied according to Equations 5-6, and the separation distance between the two Gaussians was incremented until the resulting discretized sensor output changed to a distinct value. This was taken as a lower bound on the distance between two such stimuli for them to be distinguished from a single stimulus of twice the magnitude. This procedure was repeated for 10 different locations within the sensor element (offsets from the edge in increments of 0.1) of the center of the two Gaussians, and

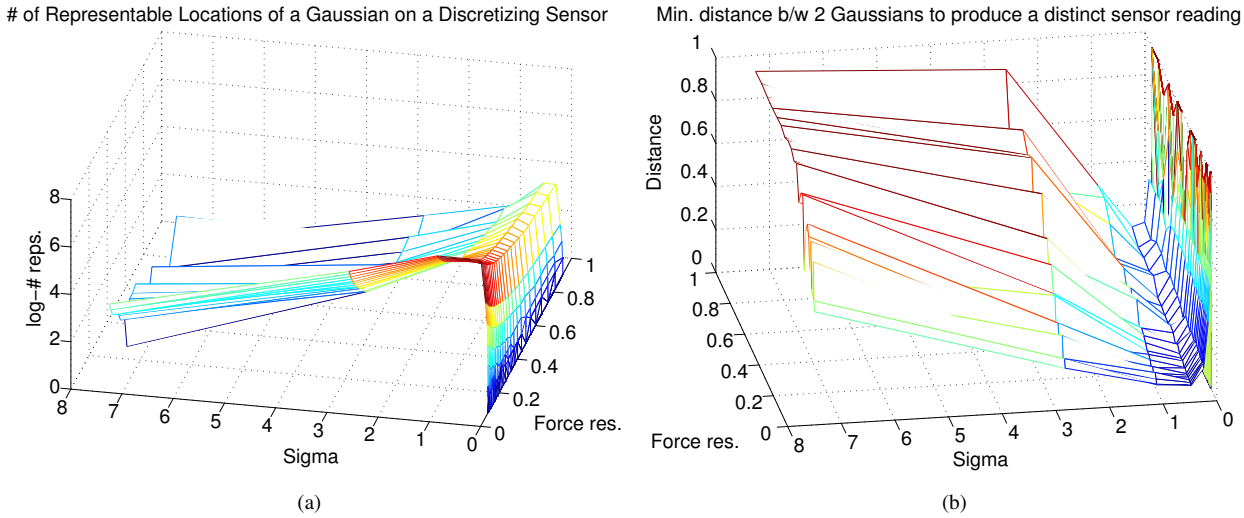

Figure 6: Spatial acuity as a function of σ, the stdev of the Gaussian point spread function: (a) The number of distinct representations produced by varying the location of the Gaussian over a single sensor element shows an optimum σ value around 0.3 for all force resolutions. (b) The minimum distance between two Gaussians which will produce a distinct sensor response from a single Gaussian shows an optimum σ close to 0.35, also independent of force resolution.

the average minimum distance was recorded. Figure 6b shows the minimum distance between the Gaussians at which that change to a distinct sensor reading occurred, again as a function of the spread of the two Gaussians and the force discretization. Once more, an optimal value occurs at $\sigma \approx 0.3$ for all force discretization levels.

Another important optimization criterion, however, is to avoid aliasing in the output. Distinct sensor readings are only useful insofar as the shape of the sensor response remains uniform as the input is translated across the sensor surface. The maximum frequency of spatial variation we should be able to detect without aliasing is the Nyquist rate of 2 sensor element widths.

A design criterion for avoiding aliasing would therefore be to choose a σ which attenuates frequencies above the Nyquist rate. Consider now the Fourier transform of a Gaussian PSF, $\mathscr{F}_x[\mathbf{G}_{0,\sigma}(x)] = \mathscr{G}(u) = e^{-2(\pi\sigma u)^2}$. If we introduce a new variable,

$$\sigma' = 1/(2\pi\sigma), \tag{8}$$

then this becomes $\mathscr{G}(u) = e^{-u^2/(2\sigma'^2)}$. The spatial Nyquist rate, in sensor element units, is $1/2$, and we desire $3\sigma' = 1/2$. This corresponds to a choice of $\sigma' = 1/6$. Substituting into equation 8 and solving for σ yields $\sigma \approx 1.0$. Since this is a lower bound on sigma, it supersedes the value of 0.3 found above. By inverting Equation 4, we see that this value is below the range of what is attainable with our strips of polyurethane, but close to the $\sigma = 1.36$ given by our thinnest available covering.

5 Simulation Method

The PSF-based modeling of tactile sensors lends itself to straightforward computational simulation. To simulate the response of the sensor, we begin with a simple deformation model. The sensor and the material covering it are viewed as a unit, and the sensor is considered to be a position-force transducer, where penetrations of the covering material are considered the input displacements.

As shown in Figure 7, there are two planes of interest for determining the sensor response: the surface of the sensing elements, and that of the deformable material covering them. An object is considered to be in contact with the sensor as soon as it collides

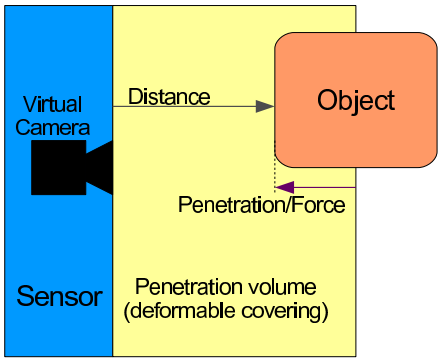

Figure 7: Simulation sensing model: a virtual camera detects distances to objects penetrating the sensor covering, then shaders convert these measurements to force readings.

with the deformable material. The object is allowed to penetrate this covering, and the penetration distance above each sensing element is then calculated. This process can be implemented efficiently using standard graphical rendering techniques. The sensor is modeled as a camera under orthographic projection, and with the viewing volume defined by the deformable surface material. The z-buffer of the rendering pipeline then provides the depth of penetration for each sensor element.

The force response function is then modeled in two steps. First, a Gaussian blur is applied to the computed penetration distances, to simulate the point spread function associated with the covering material. Then, a nonlinear function maps the resulting displacements to forces measured by the sensor. In our simulation, we have implemented these operations using OpenGL and GLSL shaders whose parameters were determined by the experiments described in Sections 3 and 2.2, respectively. As a result, we are able to achieve extremely rapid hardware rendering of tactile sensor images.

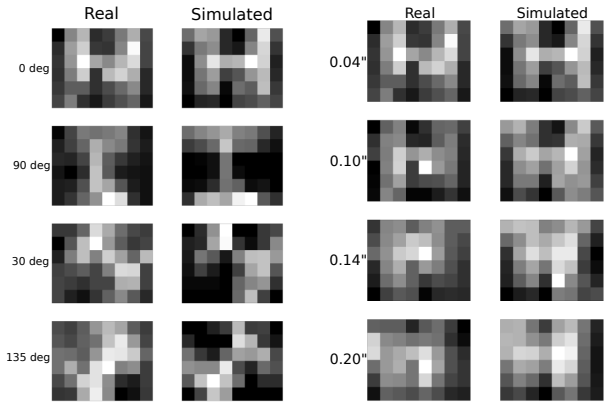

(a) Oriented H samples (b) Thickness comparison

Figure 8: Comparison of real and simulated images of an H-shaped indenter. (a) The H at several angles, all using the thinnest covering. Angles are relative to vertical. (b) The H in the same vertical orientation with each of the 4 thicknesses shows the effect of the increasing point spread. All images are scaled zero to one for readability.

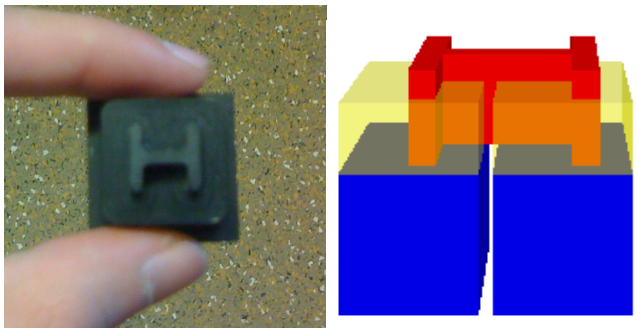

(a) (b)

Figure 9: (a) Indenter used in comparison images of Figure 8a. (b) View of 3D model of the same indenter in contact with simulated sensors. The blue blocks represent the sensors. The translucent yellow volume is their covering, which is being penetrated by the red model of the H indenter.

A comparison between the modeled response and the response of the actual sensor is depicted in Figure 8. An H-shaped indenter (Figure 9) was applied to the sensors and a 3D model of the indenter was applied to simulated sensors in the same configuration. The outputs of each are shown side-by-side, normalized (each independently) for readability. Figure 8a shows images that resulted when the indenter is applied near the center of the sensor in several different orientations, using the thinnest covering (with the smallest point-spread), and Figure 8b shows images of the indenter in the same vertical orientation, but using each covering thickness. Note the visible defocusing of the image as thickness increases, both in the real and simulated images.

Figure 10 illustrates the extensibility of the simulator and the effect of increasing the resolution of a tactile sensor. Here we compare, in simulation, the resolution of the sensors characterized in this work (PPS) with that of the human fingertip and that of another tactile sensor system, model 5027 available from Tekscan, Inc. [14]. The PPS sensors are shown as before, as an 8×6 arrangement of sensing elements, with a density of 25 sensing elements per

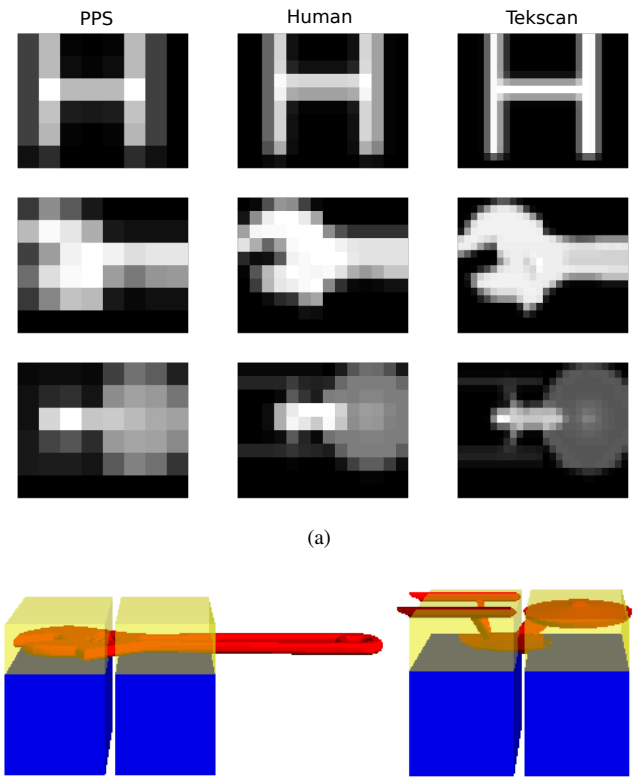

(a)

(b)

Figure 10: (a) Comparison of simulation of different-resolution sensors depressed by complex objects. Row one shows the H indenter, row two a wrench, and row three a miniature starship. Column one corresponds to the resolution of the PPS sensors, column two to that of the human finger, and column three to that of the Tekscan sensors. (b) An external view of the wrench and starship inputs. The H indenter input is shown in Figure 9b.

cm^2. The other two systems are simulated as sensors with each of their characteristic resolutions adapted to a similar aspect ratio. The innervation of Merkel receptors in the skin of the human fingertip is estimated at 70 sensors per cm^2 [15], so human sensation is simulated with a resolution of 20×14. Finally, the Tekscan system features 248 sensing elements per cm^2, and is represented by a resolution of 36×26. All three have a point spread with a σ of one sensor element width, and none have the per-element sensitivity adjustments applied in the previous simulations of the PPS sensors.

6 Discussion and Conclusions

Tactile sensors embedded beneath a compliant rubber-like covering were demonstrated to be well-approximated by a point-spread function imaging model. The point spread approximation seems to work well in the linear range of the sensor-covering system. For very large deformations, however, the response does begin to grow nonlinearly as the covering undergoes elastic hardening. Such large deformations are not encountered in typical interactions with our system. Further, the stiffness of the material used for the covering can be selected to maximize the linear range of response for the interaction forces expected.

Spatial acuity of tactile sensors was shown to be optimized by a very small point spread. Other design considerations may lead one to choose a larger spread. For example, spatial uniformity is improved with a larger point spread, as it mitigates the discontinuity

effects at sensing element boundaries. Perhaps more importantly, a larger range of object features can be imaged when using a thicker covering. Even if the goal is not to recover the physical shape of the covering surface, a thin covering limits the amount of information available for other pattern recognition applications. The preceding considerations are particularly applicable if spatial resolution is already available in abundance, as with [11] and similar sensors.

As demonstrated in Section 5, the simulation framework can be used to simulate the response of any PSF-modeled tactile sensor. Once a particular sensor has been characterized, any number of identical sensors may be replicated in simulation by simply copying the characterization parameters. Prototype algorithms can then be investigated without the need to implement them on physical hardware, or as a step in determining performance requirements on that hardware. Alternatively, the manufacturing and/or economic limitations of the current generation of tactile sensors need not apply in simulation. Therefore, arbitrarily accurate tactile sensors could be created in simulation, allowing the investigation of the effects of spatial and force resolution on tactile image processing, tactile object recognition, and tactile-based manipulation algorithms.

The ability to simulate sensor responses in real time enables a number of interesting potential extensions, including the potential to simulate active sensing of properties that may require motion to sense, such as roughness or stiffness. We do, however, currently ignore effects such as friction and other forces in directions orthogonal to the sensor surface. Additional modeling will be necessary to incorporate these effects, which will be important in some manipulation tasks, such as grasp planning or accurate simulation of surface following.

Acknowledgements

The authors thank Zhi Cheng Lai for help with programming the robotic arm and Bill Nash, Bill Quinlan, and Steven Hsiao for providing us with indenters. This work was supported in part by NSF grants #0722943 and #0748338, and a Link Foundation Fellowship for Simulation and Training.

References

[1] P. K. Allen, A. T. Miller, P. Y. Oh, and B. S. Leibowitz. Using tactile and visual sensing with a robotic hand. In *In Proc. of the 1997 IEEE Int. Conf. on Robotics and Automation*, pages 677–681, 1997.

[2] R. Bajcsy. What can we learn from one finger experiments? In *International Symposium on Robotics Research*, 1984.

[3] R. Bajcsy. *Advances in Automation and Robotics*. JAI Press, London, 1985.

[4] J. Bay. Tactile shape sensing via single- and multifingered hands. In *Robotics and Automation, 1989. Proceedings., 1989 IEEE International Conference on*, pages 290–295 vol.1, May 1989.

[5] G. Canepa, M. Morabito, D. De Rossi, A. Caiti, and T. Parisini. Shape estimation with tactile sensors: a radial basis functions approach. In *Decision and Control, 1992., Proceedings of the 31st IEEE Conference on*, pages 3493–3495 vol.4, 1992.

[6] G. Canepa, M. Morabito, D. de Rossi, A. Caiti, and T. Parisini. Shape from touch by a neural net. In *Robotics and Automation, 1992. Proceedings., 1992 IEEE International Conference on*, pages 2075–2080 vol.3, May 1992.

[7] R. Ellis and M. Qin. Singular-value and finite-element analysis of tactile shape recognition. In *Robotics and Automation, 1994. Proceedings., 1994 IEEE International Conference on*, pages 2529–2535 vol.3, May 1994.

[8] R. Fearing and T. Binford. Using a cylindrical tactile sensor for determining curvature. *Robotics and Automation, IEEE Transactions on*, 7(6):806–817, Dec 1991.

[9] W. Grimson and T. Lozano-Perez. Model-based recognition and localization from tactile data. In *IEEE International Conference on Robotics and Automation*, volume 1, pages 248–255, 1984.

[10] A. Iggo and A. R. Muir. The structure and function of a slowly adapting touch corpuscle in hairy skin. *Journal of Physiology*, 200(3):763–796, February 1969.

[11] M. K. Johnson and E. H. Adelson. Retrographic sensing for the measurement of surface texture and shape. In *Computer Vision and Pattern Recognition (CVPR)*, pages 1070–1077, 2009.

[12] PPS. DigiTacts II^{TM}, tactile array sensor evaluation kit with digital output. Pressure Profile Systems. Available from: <http://www.pressureprofile.com/UserFiles/File/DigiTactsII%20Evaluation%20Specification%20Sheet.pdf>.

[13] M. Shimojo. Spatial filtering characteristic of elastic cover for tactile sensor. In *Robotics and Automation, 1994. Proceedings., 1994 IEEE International Conference on*, pages 287–292 vol.1, May 1994.

[14] TekScan. Sensor map #5027. TekScan Inc. Available from: <http://www.tekscan.com/industrial/catalog/5027.html>.

[15] A. . Vallbo and R. Johansson. Properties of cutaneous mechanoreceptors in the human hand related to touch sensation. *Human Neurobiology*, 3:3–14, 1984.

[16] Y. Yanagida, M. Kakita, R. Lindeman, Y. Kume, and N. Tetsutani. Vibrotactile letter reading using a low-resolution tactor array. *Haptic Interfaces for Virtual Environment and Teleoperator Systems, 2004. HAPTICS '04. Proceedings. 12th International Symposium on*, pages 400–406, March 2004.